Use of SiO_2 nanoparticles as etch mask to generate Si nanorods by reactive ion etch

Eih-Zhe Liang, Chao-Jei Huang, and Ching-Fuh Lin[a)]
Graduate Institute of Electro-optical Engineering, National Taiwan University, Taipei 106, Taiwan

(Received 26 July 2005; accepted 9 January 2006; published 17 February 2006)

Silicon nanorods 20 nm in diameter are fabricated by reactive ion etch (RIE) to study anisotropy and damage profile in decananometer scale. RIE of gas mixture of SF_6/O_2 and SF_6/CHF_3 is tuned to achieve high anisotropy. The gas specie of SF_6/O_2 can reach 90% anisotropy, 84° taper angle, and 10:1 selectivity when SiO_2 is used as the etching mask. The gas species of SF_6/CHF_3 can reach 95% anisotropy, 87° taper angle, and 10:1 selectivity with Cr as the mask. The fabrication technique of nanorods uses a monolayer of silicon dioxide nanoparticle as the etching mask. The nanorods uniformly cover up the entire 2 in. wafers with high density of 2×10^{11} cm^{-2}. Surface damage after the etching process of nanostructures is monitored using the microwave-reflectance photoconductance decay with KOH removal-and-probe technique. Highly damaged silicon is found within a depth of 30 nm and the lightly damaged part extends more than 100 nm. © *2006 American Vacuum Society.* [DOI: 10.1116/1.2172251]

I. INTRODUCTION

Decananometer structures on silicon are important features for nanoelectronics, nanophotonics, and their integration; for example, sub-50 nm channels in fin field effect transistor (FinFET),[1,2] sub-30 nm islands in a single electron transistor (SET),[3,4] sub-30 nm Si nanoparticles with light emission[5,6] and optical gain,[7] sub-100 nm structures in photonic-band gap devices,[8,9] subwavelength antireflection structures in Si optical components,[10,11] and so on. To achieve small feature size and wide-area uniformity in highly productive fabrication of decananometer structures, reactive ion etch (RIE) is a good choice of dry-etch technology.

However, although anisotropy of submicrometer structure on silicon has been an extensive research topic,[12,13] it has not been clearly known if RIE can be applied to mass production of decananometer structures. In this work, we demonstrate silicon nanorods with 20 nm feature size on single-crystalline Si wafers by RIE. The structures are closely packed with 50 nm pitch and almost uniformly cover up the entire 2 in. wafers with nanorods at a high density of 2×10^{11} cm^{-2}. Our results show both the scalability of the RIE technique on decananometer structures and the reproducibility over wafer scale area.

In the fabrication of high-density nanostructures, one performance issue arises during shrinkage of device size into the decananometer scale. Large surface to volume ratio makes the quality of the etched surface influential to device performance in electronic[14] and optical[15] aspects. Surface damage of the wafers caused by ion bombardment during RIE is inevitable, but can be minimized if a monitoring tool is at hand. Here the etching damage of produced nanorods is monitored by microwave-reflection photoconductance decay (MWPCD) with a removal-and-probe technique. This method can produce a sensitive damage profile with decananometer resolution.

II. ANISOTROPY CONTROL

In our experiments, high anisotropy is first investigated in submicrometer structures and then adjusted to decananometer structures. RIE takes place at the Plasmalab 80Plus (Oxford Instrument). The lower electrode is a graphite plate of 240 mm diameter. Two gas species, SF_6/O_2 and SF_6/CHF_3, are used to etch silicon wafers with different types of masks for testing anisotropic recipes. The gas specie of SF_6/O_2 can reach 90% anisotropy, 84° taper angle, and 10:1 selectivity when SiO_2 is used as the etching mask. The anisotropy (AI) here is defined as $AI=1-V_L/V_H$, where V_L is the laterally etched width and V_H is the vertically etched depth. The taper angle, the angle between the sidewall and horizontal plane, is then given by $\cot^{-1}$ (1-AI). Another gas species of SF_6/CHF_3 can reach 95% anisotropy, 87° taper angle, and 10:1 selectivity with chromium as the mask. The latter gas species has the same high anisotropy but with only 1:1 selectivity when polymer or oxide is used as the etching mask. These two gas species are investigated for common use of silicon dioxide as a positive pattern transfer and chromium as a negative pattern transfer through the liftoff process.

The etch profile is shown in Fig. 1. It can be seen that the SF_6/O_2 etch will not produce undercut underneath the etching mask until the etch depth is greater than 200 nm. SF_6/CHF_6 gases produce nearly no undercut. This gas specie also results in a steeper profile rather than the species of SF_6/O_2 gases, but with less etching rate. The relation of etching rate and anisotropy is shown in Fig. 2. The anisotropy is only affected by gas ratio and gas pressure. It is less variable with rf power in range of 50–120 W. This is due to different sidewall passivation with different gas partial pressure. The etching rate is strongly influenced by rf power and SF_6 gas partial pressure, since SF_6 is the major etching gas.

[a)]Author to whom correspondence should be addressed; also with Department of Electrical Engineering and Graduate Institute of Electronics Engineering; electronic mail: cflin@cc.ee.ntu.edu.tw

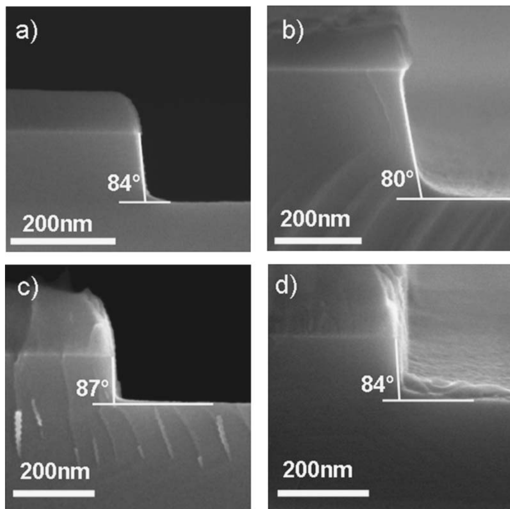

FIG. 1. Etching profile (a) $SF_6:O_2=10:25$ P 10 mTorr/120 W (anisotropy 90%, 84° taper angle); (b) $SF_6:O_2=15:25$ P 10 mTorr/120 W (anisotropy 82%, 80° taper angle); (c) $SF_6:CHF_3=2:50$ P 10 mTorr/120 W (anisotropy 95%, 87° taper angle); and (d) $SF_6:CHF_3=3:25$ P 10 mTorr/120 W (anisotropy 90%, 84° taper angle).

Its etching rate depends strongly on its concentration, i.e., gas partial pressure, and bombardment energy, increased by raising the rf power.

It is known that SF_6 has isotropy etch of silicon, and O_2 is added to passivate the sidewall to achieve anisotropy.[16] The main etching mechanism is the rf power activated formation of gaseous SiF_x. With lower SF_6 percentage and higher content of oxygen, anisotropy is better, etching rate is lower, and the etched profile has less undercut. Increasing rf power enhances reactivity of SF_6 and raises the etching rate. Gas pressure has a complicated influence on the etching rate and anisotropy.[17] Etching rate is increased by raising the total gas pressure, but the experiment has shown that anisotropy only occurs under a pressure of 50 mTorr. All conditions presented here are obtained under 10 mTorr pressure.

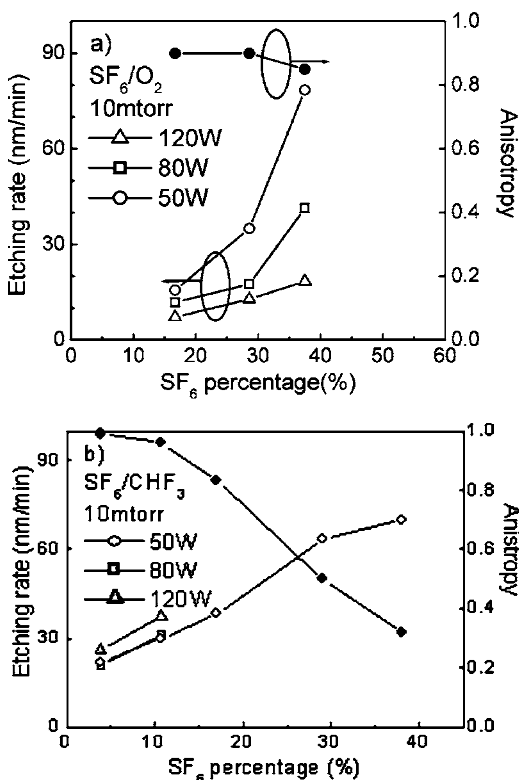

FIG. 2. Etching rate and anisotropy vs gas mixture ratio of: (a) SF_6/O_2 and (b) SF_6/CHF_3.

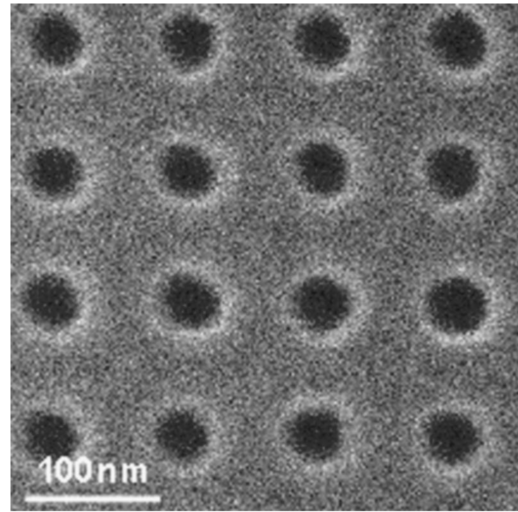

FIG. 3. E-beam pattern, etched silicon of 50 nm pore with 100 nm pitch, estimated depth of 150 nm.

For the SF_6/CHF_3 case, CHF_3 will form a productive carbon–silicon complex at the sidewall.[13] The major reason for introducing isotropic SF_6 etching is to reduce roundness between the sidewall and etched plane. This increases penetration capability in etching through decananometer pores or trenches. The relation of etching rate to rf power is the same as in the SF_6/O_2 case for increasing reactivity of CHF_3. The reduction of the SF_6 portion improves the anisotropic but does not affect the etching rate much because CHF_3 is the main etchant. The pressure is maintained at 10 mTorr to keep good SF_6 reactivity, but still with great anisotropy.

The etching recipes are then applied to the resist mask for electron beam lithography to test the anisotropy in 50 nm structures. The mask is ZEP520A with 360 nm thickness. The pattern is a 50 nm periodic pole with 100 nm pitch. It is etched using SF_6/CHF_3 gases with 95% anisotropy and 87° taper angle to yield silicon poles of 150 nm depth. The scanning electron microscope (SEM) photo of the etched silicon poles is shown in Fig. 3. The poles have a 55 nm diameter, which is a 5% widening of the resist pore mask at the single sidewall.

III. ETCH MASK PREPARATION

Since the etching recipe is proved to work on the 50 nm resist mask, it is subsequently applied to test anisotropy with a 20–30 nm dia. mask of silicon dioxide nanoparticle. The SiO_2 nanoparticles are colloidal silica originally dispersed in

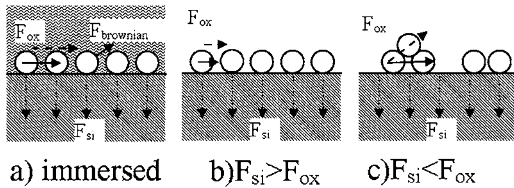

FIG. 4. Forces diagram of nanoparticles (a) immersed in solution, (b) monolayer, and (c) clustering in spin-coated layer.

methanol (commercially available from Nissan Chemical with the stock-name MA-ST-M). The original SiO_2 nanoparticles in methanol have a weight percentage of 40%–41%. The SiO_2 nanoparticles have a sphere shape with 20–30 nm diameter. SiO_2 nanoparticles in methanol with such a high weight percentage cannot be directly used as the etch mask. They have to be diluted before being deposited onto the Si wafer. Fortunately, the viscosity of the solution can be varied when it is further dispersed with isopropanol. Then nearly a monolayer of SiO_2 nanoparticle can be applied onto the Si wafer to function as the etch mask for the decananometer feature size and uniform wafer-scale coverage. However, the formation of SiO_2 nanoparticle monolayers on the silicon surface is not easy to obtain. The spin-coated method and its principles are described as follows.

The SiO_2 nanoparticles are further dispersed in isopropanol to have the diluted concentration of 1% in weight. The silicon wafer is treated with buffered oxide etch (BOE), ($HF:NH_4F=1:6$) to remove native oxide and preserve a hydrophobic surface. The nanoparticle solution is heated above 50 °C and applied to the silicon surface by spin coating. The function of raised room temperatureis to reduce the mutual attraction of nanoparticles by enhancement of Brownian motion in the solution. As schematically shown in Fig. 4(a), the relative magnitude of the attraction force between adjacent nanoparticles F_{ox} and the attraction between nanoparticle and the silicon surface F_{si} will lead to different morphology. When $F_{si} > F_{ox}$, shown in Fig. 4(b), the spin-coated layer is a monolayer. It is measured to be 25 nm in thickness with an effective refractive index of 1.46, measured by an ellisometer at 633 nm. When $F_{si} < F_{ox}$, shown in Fig. 4(c), nanoparticles become clustering and the spin-coated layer cannot form long-range film within the submicron area. To obtain a uniform monolayer of SiO_2 nanoparticles across the 2 in. wafer, solvents with high viscosity like isopropanol, raised temperature, and adequate solution concentration are required.

IV. SILICON NANORODS

After the etch mask is prepared, the wafer is placed in the RIE chamber and a dry etch is performed. SF_6/O_2 or SF_6/CHF_3 etch can be used. The SEM photo (top view) of an as-spun silicon dioxide nanoparticle mask is shown in Fig. 5(a). The lateral arrangement is random because the SiO_2 nanoparticles have a large size dispersion of 40%. However the nanoparticles do form a monolayer without clustering. The packing density is counted to be 2×10^{11} cm^{-2}.

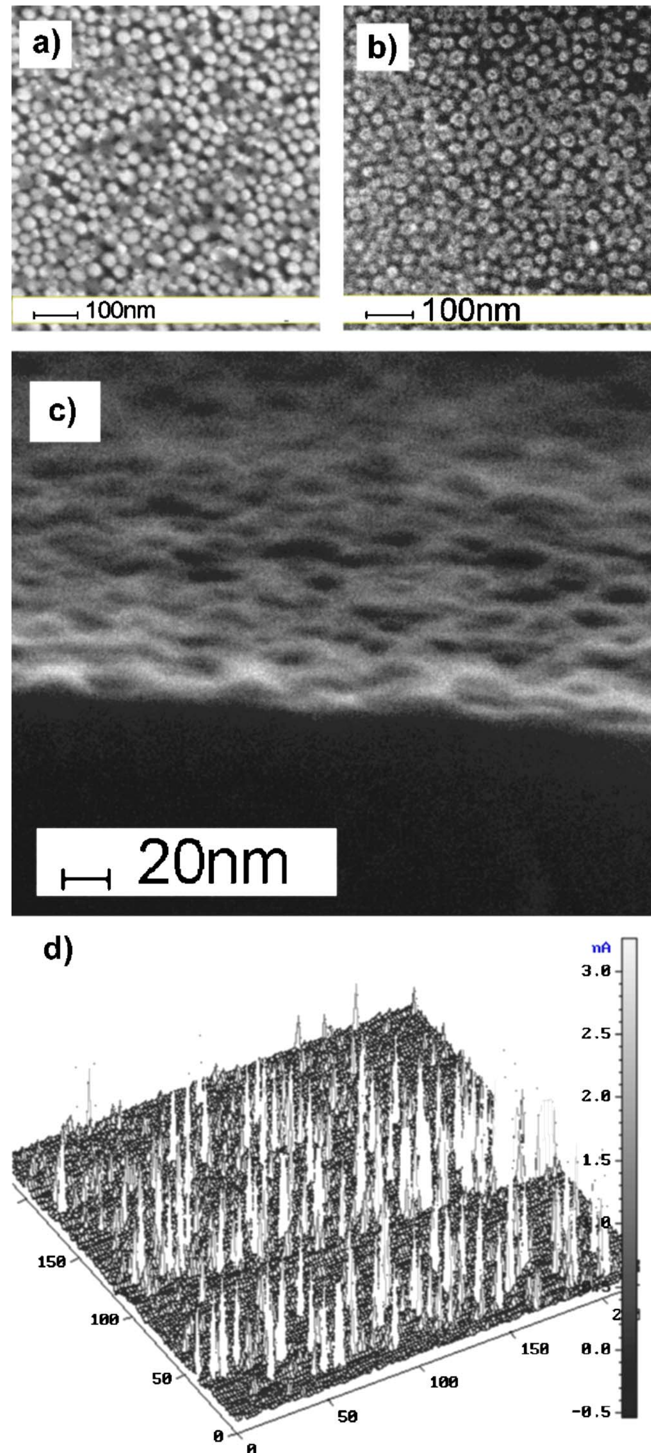

FIG. 5. (a) SEM image of silicon dioxide nanoparticles spin-coated film; (b) silicon nanorods with average diameter size 20 nm (top view); (c) (side view); and (d) STM image with current feedback mode.

After the RIE process, the etched wafer is treated with hydrofluric acid (HF 49%) to remove the SiO_2-nanoparticle mask and shown in Figs. 5(b) and 5(c). The silicon nanorods have a diameter of 20 nm and a height of 20 nm. The pitch, defined as the mean spacing of adjacent nanorods, is 50 nm. The separation trench of two nanorods is 5 nm wide. From the top view of the etched silicon nanorods, high anisotropy

preserves the locally spherical shape of the SiO_2 nanoparticle mask. The side view shows that masked nanorods have the same height. The nanorods have a trapezoidal shape and the top is slightly rounded due to the pattern transfer of the locally spherical shape of the mask.

To prove the masked top is not etched at all, scanning tunneling microscopy (STM) is taken at a constant height with the tunneling current measured. The STM result is shown in Fig. 5(d). With this sensitive method, the tunneling current has a peak at each top of the nanorods. The peak current shows the same range of magnitude over a wide area. The small variation of the peak current indicates that the height variation of the created nanorods is also small. The reason is because no undercut in this recipe of RIE has resulted even with the loose coverage of SiO_2 nanoparticles on the Si surface.

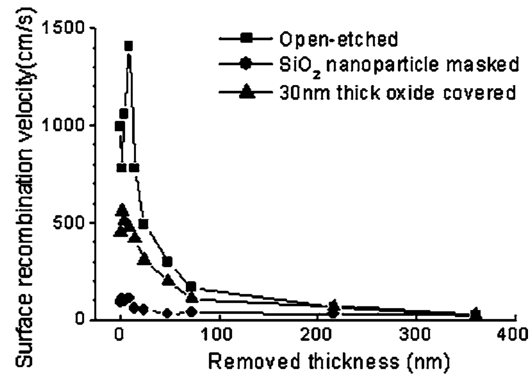

FIG. 6. Derived surface recombination velocity of damaged front side of open-etched wafer (square, SF_6/O_2 dry etch at the pressure of 10 mTorr and the rf power of 120 W), SiO_2 nanoparticle masked wafer, 30 nm thick oxide covered wafer, vs different removed thickness by KOH wet etch.

V. ETCH DAMAGE

The damage profile of the etched wafer is monitored by MWPCD[18] by the KOH etch-and-probe method. With controlled damage, RIE can be further applied to create a lattice-quality-sensitive decananometer structure like SET, light emitter, solar cell, or photodetector. MWPCD measures the charge carrier lifetime of silicon wafers. The measured minority carrier lifetime is a joint parameter of surface recombination center and bulk trap from ion bombardment defects. By removal of the damaged part at the surface, the carrier lifetime will increase gradually to the value of an unetched wafer. The relation of the inverse of the lifetime, or effective surface recombination velocity, to the removal depth shows how deep the ion penetrates into the lattice.

It is known that reactive ion etch has polymeric surface contamination and lattice damage due to reactive ion bombardment. The surface is modified into complex bonding, for example, Si–F and Si–O bonding in SF_6 and O_2 gas ambients. This kind of contamination layer is estimated to be as shallow as 5–8 nm.[19] On the other hand, the lattice damage is deeper since the reactive ion penetrates into the inner crystal. 16–36 nm thickness of damage was reported previously.[19]

As for the damaged profile, the lower gas pressure results in less probability of ion bombardment. As a result, the total damage defect density of the etched wafer is reduced under the same rf power. Since the lower gas pressure is needed to have the higher anisotropy, the lower defect density and lower surface recombination velocity is expected. The thickness of damage layer, however, depends on the penetration depth of the reactive ion.[20] It could be much more influenced by the rf power than by the gas pressure.

Here, a one-side polished float zone silicon wafer with the (100) orientation and doping $\sim 10^{-15}$ cm^{-3} is used. Its carrier lifetime is measured by MWPCD with the sample immersed in 8% molar iodine/methanol.[18] The microwave probe is at 10 GHz. The excitation source is the second harmonic generation at 532 nm from Nd:yttrium–aluminum–garnet pulse laser with the excitation intensity up to 400 kW/cm^2. The wafer has a thickness of 525 μm and the charge carrier lifetime of the unetched wafer is 1.3 ms.

To evaluate the etch damage, the wafer is first open etched, i.e., uncovered by any mask, with the aforementioned SF_6/O_2 dry etch at the pressure of 10 mTorr and the rf power of 120 W and then the carrier lifetime of the etched sample is measured. The sample is dry etched for 80 s with an etching depth of 20 nm. Afterward, the damage depth is investigated by removing the top surface of the etched sample using the KOH solution for a certain depth and then the carrier lifetime is measured again. The surface silicon is removed using KOH (45% in weight) wet etch at 35 °C with an etching rate of 2.1 nm/s.[21] After the removal of the presumed damage depth is reached, the wafer is rinsed by deionized water and placed into iodine/methanol. Its carrier lifetime is measured using MWPCD. Then it is placed back in the wet etch bath again for further etching and lifetime measurement. The measured lifetime τ_{PCD} can be expressed[18] by

$$\frac{1}{\tau_{PCD}} = \frac{1}{\tau_{BULK}} + \frac{S_1 + S_2}{W}, \quad (1)$$

where τ_{BULK} is the bulk lifetime, W is the wafer thickness, and S_1 and S_2 are surface recombination velocities of damaged front side and undamaged backside, respectively. Please note that S_2 is very small, <50 cm/s, determined before the dry etch. S_1 is then calculated from τ_{PCD}, τ_{BULK}, and W. The derived surface recombination velocity versus the removed thickness is shown in Fig. 6 (square). We can see that the highly damaged silicon is about 30–40 nm deep. In addition, this sensitive measurement suggests that some lightly damaged part extends into more than 100 nm.

To examine the damage of the decananometer structure, Si nanorods, the MWPCD comparison of etch damage in the Si wafer covered with SiO_2 nanoparticle (circle) and a 30 nm thick evaporated oxide (triangle) are also plotted in Fig. 6. The comparison leads two observations. First, the wafer covered with 30 nm thick evaporated oxide shows no significant increase in surface recombination velocity. Therefore SiO_2 of

30 nm thickness is sufficient to prevent from surface damage in 80 s etching time. Second, the SiO_2 nanoparticle masked wafer has approximately the same depth of etch damage but less surface recombination velocity at the surface than the open-etched wafer. This means the SiO_2 nanoparticle masked wafer suffered less RIE damage. The two observations suggest that the reactive ion cannot penetrate through SiO_2 nanoparticles with 20–30 nm diameter in the vertical direction in the creation of Si nanorods. On the other hand, the sidewall of the Si nanorods is not protected with any mask, but is not directly bombarded by the dry-etching ions, either. Thus, the damage to the sidewall is not as bad as the unmasked top surface. Because the damage to the sidewall of the Si nanorods cannot be directly measured, it is evaluated as follows. Assume that the ion penetration depth is linearly proportional to the reactivity of the etching gas. Considering 90% anisotropy of our Sf_6/O_2 recipe, the sidewall damage is thus estimated to be 10% of the vertical damage. In this case, the side damage is about 3 nm deep. Therefore, the inner part of the 25 nm nanorods will still preserve its original good quality.

VI. CONCLUSION

We demonstrate high anisotropy and damage monitoring of reactive ion etch in the creation of decananometer structures. RIE of gas mixture of SF_6/O_2 and SF_6/CHF_3 is tuned to have high anisotropy of 90% and 95%, respectively. The gas specie of SF_6/O_2 can reach 90% anisotropy, 84° taper angle, and 10:1 selectivity when SiO_2 is used as the etching mask. The gas species of SF_6/CHF_3 can reach 95% anisotropy, 87° taper angle, and 10:1 selectivity with Cr as the mask. To prove its applicability to decananometer structure, silicon nanorods of 20 nm diam size are created. These two recipes of RIE are carried out over a 2 in. wafer and demonstrated uniform etching result. A silicon dioxide nanoparticle monolayer is used as the mask. The Si created nanorods distribute uniformly over the entire 2 in. wafers with a high density of 2×10^{11} cm^{-2}. Surface damage after the etching process of nanostructures is monitored using MWPCD with the KOH removal-and-probe technique. In the investigation of the etched silicon, the highly damaged part is found within a depth of 30 nm and the lightly damaged part extends into more than 100 nm. Sidewall damage is also investigated. The 3 nm lateral damage depth of nanorods is estimated due to the etching process.

ACKNOWLEDGMENT

This work is supported partly by the National Science Council of Taiwan under Contract Nos. NSC 94-2120-M-002-010 and NSC 93-2112-M-002-009.

[1]B. Y. Tsui and C. P. Lin, IEEE Electron Device Lett. **25**, 430 (2004).
[2]X. Huang *et al.*, IEEE Trans. Electron Devices **48**, 880 (2001).
[3]H. Namatsu, Y. Watanabe, K. Yamazaki, T. Yamaguchi, M. Nagase, T. Ono, A. Fujiwara, and S. Horiguchi, J. Vac. Sci. Technol. B **21**, 1 (2003).
[4]Y. Ono, Y. Takahashi, K. Yamazaki, M. Nagase, H. Namatsu, K. Kurihara, and K. Murase, IEEE Trans. Electron Devices **47**, 147 (2000).
[5]S. Lee, W. Cho, J. Woon, I. Han, C. Ki, J. Won, and J. I. Lee, Phys. Status Solidi C **1**, 2767 (2004).
[6]Z. Yaniv, L. Thuesen, D. Hutchins, and R. L. Fink, Proceedings 2002 SID Conference Record of the International Display Research Conference (France, 2002), p. 753–754.
[7]K. Luterova *et al.*, Opt. Mater. (Amsterdam, Neth.) **27**, 750 (2005).
[8]P. K. Kashkarov, L. A. Golovan, A. B. Fedotov, A. I Efimova, L. P. Kuznetsova, V. Y. Timoshenko, D. A. Sidorov-Biryukov, A. M. Zheltikov, and J. W. Haus, J. Opt. Soc. Am. B **19**, 2273 (2002).
[9]H. Sun, W. Shi, and Y. J. Ding, Proceedings of 2003 Lasers and Electro-Optics Society Annual Meeting, 2003, Vol. 2, p. 942.
[10]Z. Yu, H. Gao, W. Wu, H. Ge, and S. Y. Chou, J. Vac. Sci. Technol. B **21**, 2874 (2003).
[11]K. Hane and Y. Kanamori, Proceedings 2001 Pacific Rim Conference on Lasers and Electro-Optics Technical Digest (Japan, 2001), p. I186–I187.
[12]S. Grigoropoulos, E. Gogolides, A. D. Tserepi, and A. G. Nassiopoulos, J. Vac. Sci. Technol. B **15**, 640 (1997).
[13]E. Gogolides, S. Grigoropoulos, and A. G. Nassiopoulos, Microelectron. Eng. **27**, 449 (1995).
[14]C. F. H. Gondran, E. Morales, A. Guerry, W. Xiong, C. R. Cleavelin, R. Wise, S. Balasubramanian, and T.-J. King, Mater. Res. Soc. Symp. Proc. **811**, 365 (2004).
[15]F. Llopis and I. Tobias, Prog. Photovoltaics **13**, 27 (2005).
[16]T. Syau, B. Baliga, H. Jayant, and W. Raymond, J. Electrochem. Soc. **138**, 3076 (1991).
[17]I. W. Rangelow, J. Vac. Sci. Technol. A **21**, 1550 (2003).
[18]A. W. Stephen and M. A. Green, Sol. Energy Mater. Sol. Cells **45**, 255 (1997).
[19]K. A. Reihardt and S. M. Kelso, Proc. SPIE **2638**, 147 (1995).
[20]K. A. Valiev, *The Physics of Submicron Lithography* (Plenum, New York, 1992), pp. 237–239.
[21]L. D. Dyer, G. J. Grant, C. M. Tiption, and A. E. Stephens, J. Electrochem. Soc. **136**, 3016 (1989).